Research Square

Preprints are preliminary reports that have not undergone peer review.
They should not be considered conclusive, used to inform clinical practice,
or referenced by the media as validated information.

Heterogeneity of Senescence-Associated Signatures in Osteoarthritic Chondrocytes Revealed Under Physiologic and Hyperoxic Oxygen Tensions

Jorge Fernandez Davila
University of North Carolina
Makayla Poindexter
University of North Carolina
Anna Pato
University of North Carolina
Seyoun Byun
University of North Carolina
Jacqueline Shine
University of North Carolina
Christopher Olcott
University of North Carolina
Hadi Pourhadi
Wake Forest University
Jingyun Lee
Wake Forest University
Douglas Phanstiel
University of North Carolina
Brian Diekman
University of North Carolina
Richard Loeser, MD
richard_loeser@med.unc.edu
University of North Carolina

Research Article

Keywords:

Posted Date: November 12th, 2026

DOI: https://doi.org/10.21203/rs.3.rs-11354432/v1

License: This work is licensed under a Creative Commons Attribution 4.0 International License.
Read Full License

Additional Declarations: No competing interests reported.

Heterogeneity of Senescence-Associated Signatures in Osteoarthritic Chondrocytes Revealed Under Physiologic and Hyperoxic Oxygen Tensions

Jorge G. Fernandez Davila[1], Makayla J. Poindexter[1], Anna Pato[1], Seyoun Byun[2], Jacqueline Shine[1], Christopher W. Olcott[3], Hadi Pourhadi[4], Jingyun Lee[4] Douglas H. Phanstiel[1,2,5], Brian O. Diekman[1,6], Richard F. Loeser[1,7].

[1] Thurston Arthritis Research Center, University of North Carolina School of Medicine, Chapel Hill, NC, USA.

[2] Curriculum in Bioinformatics and Computational Biology, University of North Carolina, Chapel Hill, NC, USA.

[3] Department of Orthopedics, University of North Carolina School of Medicine, Chapel Hill, NC, USA.

[4] Department of Internal Medicine, Wake Forest University School of Medicine, Winston-Salem, NC, USA.

[5] Department of Cell Biology and Physiology, University of North Carolina School of Medicine, Chapel Hill, NC, USA.

[6] Lampe Joint Department of Biomedical Engineering, University of North Carolina and North Carolina State University, Raleigh, NC, USA.

[7] Division of Rheumatology, Allergy and Immunology, University of North Carolina School of Medicine, Chapel Hill, NC, USA.

Running Title: Senescence enrichment signatures in osteoarthritic chondrocytes

Corresponding author:

Richard F. Loeser

University of North Carolina

3300 Thurston Building

Campus Box 7280

Chapel Hill, NC 27599-7280

E-mail: richard_loeser@med.unc.edu

E-mail: jfernan@email.unc.edu

E-mail: makayla_poindexter@med.unc.edu

E-mail: anna_pato@med.unc.edu

E-mail: sbyun@unc.edu

E-mail: yalins@med.unc.edu

E-mail: hadi.pourhadi@advocatehealth.org

E-mail: jingyun.lee@advocatehealth.org

E-mail: chistopher_olcott@med.unc.edu

E-mail: douglas_phanstiel@med.unc.edu

E-mail: bdiekman@email.unc.edu

Abstract

Background

Osteoarthritis (OA) is associated with cellular senescence and the accumulation of cells with the senescence-associated secretory phenotype (SASP) that may contribute to disease progression. However, methods for identifying senescent chondrocytes remain poorly defined. This study used multi-omics to characterize the senescence phenotype of OA chondrocytes cultured under physiologic and room air culture conditions.

Methods

Chondrocytes isolated from knee OA donors (n=14) were treated with doxorubicin for 9 days under hyperoxic (21% O_2) or physiological (3% O_2) oxygen conditions to enrich cultures for senescent cells. Senescence was assessed using standard senescence markers (CDKN1A, CDKN2A, and SA-β-gal) and by RNA-seq. Senescence signatures were evaluated using SenCID, DeepScence, and hUSI. Top-ranked genes from DeepScence and hUSI were compared with the SenMayo senescence gene set to identify candidate genes associated with senescence in OA chondrocytes. Proteomics analysis of conditioned media was used to identify SASP factors. Normal chondrocytes treated with the SASP factor GDF15 were evaluated using RNAseq.

Results

Doxorubicin increased senescence markers p21 and p16 and SA-β-gal. Transcriptomic responses differed between oxygen conditions, with pathway analysis

identifying senescence-related Hallmark and Reactome pathways. SenCID, DeepScence, and hUSI produced distinct senescence scores, indicating heterogeneity in transcriptional senescence signatures. Comparison of the top-ranked genes from DeepScence and hUSI with the SenMayo gene set identified 47 genes shared by two or more groups. GDF15 was the most highly secreted SASP factor under both oxygen conditions. Treatment of normal chondrocyte with physiological concentrations of GDF15 did not induce senescence-associated transcriptional programs but rather decreased expression of inflammatory genes.

Conclusion

OA chondrocytes exhibit heterogeneous senescence phenotypes that are influenced by oxygen tension, supporting the use of multiple complementary approaches rather than a single senescence marker. Nuclear p21 and p16, transcriptomic scoring, and secretome profiling provided distinct information about the senescent phenotype. GDF15 emerged as a prominent chondrocyte SASP factor but it appeared to function as a negative regulator of inflammation rather than as a contributing factor. Integration of senescence-associated datasets also enabled the development of a chondrocyte-relevant gene signature that may improve transcriptional assessment of senescence in OA chondrocytes.

Introduction

Osteoarthritis (OA) is a chronic, whole-joint disease characterized by progressive cartilage loss, chronic inflammation, pain, and functional impairment[1,2]. Aging is a major risk factor for OA as well as for numerous chronic conditions, including cardiovascular disease, diabetes, fibrosis, and neurodegenerative disorders such as Alzheimer's disease. A central mechanism implicated in age-related diseases is cellular senescence, a state of stable cell-cycle arrest accompanied by extensive phenotypic and functional alterations[3,4]. Senescent cells are commonly characterized by increased expression of cell-cycle inhibitors, such as p16 and p21, that contribute to cell cycle arrest, often in response to DNA and/or other macromolecular cellular damage. Senescent cells contribute to tissue pathology through the acquisition of a senescence-associated secretory phenotype (SASP)[3,4]. The SASP comprises a diverse, context-dependent array of inflammatory cytokines, chemokines, growth factors, proteases, and other secreted factors that can alter the local tissue microenvironment and promote chronic inflammation and tissue dysfunction[5]. Importantly, the composition and magnitude of the senescent phenotype and SASP can vary substantially across cell types, tissues, inducers, and microenvironments, suggesting that senescence is not a uniform cellular state[6,7].

Chondrocytes are the primary resident cells of articular cartilage and are responsible for maintaining the balance between extracellular matrix synthesis and degradation. During OA, chondrocytes undergo profound phenotypic changes that promote matrix catabolism and inflammatory signaling[2,8]. Cellular senescence has been implicated as one of these disease-associated phenotypes, with senescent or

senescent-like chondrocytes identified in human OA cartilage and experimental models of OA[9]. Senescent chondrocytes can produce SASP factors that include inflammatory mediators and matrix-degrading enzymes, such as the matrix metalloproteinases (MMPs), potentially contributing to both cartilage destruction and the inflammatory joint microenvironment. However, the molecular and secretory characteristics of senescent chondrocytes remain incompletely defined.

A challenge in studying basic mechanisms contributing to cellular senescence is that senescent cells often represent a small proportion of the cell population in a given tissue[10]. For *in vitro* studies, cell cultures are often enriched for senescent cells using methods that seek to recapitulate core inducers of senescence *in vivo,* such as causing DNA damage or generating oxidative stress. Due to the heterogeneity observed in senescence, the induction of senescence-associated gene expression and secretory profiles identified in one tissue or cell type may not accurately represent senescence in another[6,7].

Another condition that is often overlooked in cell culture studies of senescence, as well as many other areas of basic cellular research, is the oxygen concentration under which the cells are cultured. This is particularly relevant to articular chondrocytes that reside within a relatively hypoxic cartilage environment. Oxygen concentrations within articular cartilage are substantially lower than those used in conventional cell culture, with chondrocytes experiencing oxygen concentrations generally ranging from approximately 2–6% depending on tissue depth and physiological conditions[11]. In contrast, standard cell culture is performed in room air at approximately 21% oxygen, a condition that is considerably more oxygen-rich than the native cartilage environment

and may influence cellular metabolism, stress responses, and senescence-associated phenotypes. Thus, incorporating physiologically relevant oxygen conditions is an important consideration for accurately characterizing chondrocyte senescence.

Doxorubicin is a chemotherapeutic agent that intercalates with DNA, serves as a topoisomerase poison, and generates reactive oxygen species (ROS) through mitochondrial dysfunction[12]. Doxorubicin has been widely used with chondrocytes and other cell types to induce cellular senescence via persistent DNA damage and activation of cell-cycle arrest[13]. However, many experimental models of chondrocyte senescence have relied on relatively short induction periods of acute cellular stress, which may not fully capture the sustained transcriptional and secretory phenotypes associated with long-term senescence. Furthermore, the influence of oxygen availability on the development and phenotype of induced senescence in human chondrocytes has not been fully characterized. Therefore, a more comprehensive characterization of chondrocyte senescence under physiologically relevant oxygen conditions may provide insight into the molecular programs and secreted factors associated with this disease-relevant cellular state.

In this study, we used doxorubicin to enrich for senescence in human articular chondrocytes isolated from OA joint tissue and cultured at either 3% oxygen, representing a physiologically relevant cartilage environment (normoxia), or 21% oxygen, representing conventional tissue culture conditions and a relatively hyperoxic environment. We characterized the cellular response at the transcriptomic and secretory levels by performing RNA sequencing and proteomic analysis of conditioned media, respectively. This approach allowed us to examine both gene expression programs and

extracellular secretome changes associated with chondrocyte senescence and to determine how these responses were influenced by oxygen concentration.

Finally, because commonly used senescence markers and gene signatures may not fully capture the heterogeneous and cell-type-specific nature of senescence, we evaluated three computational senescence scoring approaches: Senescent cell identification (SenCID)[14], the human universal senescence index (hUSI)[15], and DeepScence[16] to assess their ability to identify senescence-associated transcriptional programs in chondrocytes. We also compared the results of these scoring systems to the widely studied SenMayo gene set[17]. Rather than assuming that canonical senescence markers are universally applicable across tissues, we used these approaches to identify transcriptional programs and candidate genes associated with the senescent phenotype in human chondrocytes. Collectively, these studies provide a transcriptomic and proteomic characterization of chondrocyte senescence under distinct oxygen environments and identify molecular features that may improve senescence characterization in OA cartilage.

Methods

Tissue procurement, cell isolation, and culture

OA chondrocytes were isolated from cartilage obtained from patients undergoing total knee arthroplasty (n=14) at the University of North Carolina Hospital (UNC), Hillsborough, NC. Normal chondrocytes were isolated from non-OA talar cartilage obtained from deceased donors (n=4) through the Gift of Hope Organ and Tissue Donor

Network (Itasca, IL) and Rush Medical Center (Chicago, IL). Donor demographics are provided in Supplementary Table 1.

Articular chondrocytes were isolated from cartilage tissue by enzymatic digestion and expansion in monolayer culture as previously described[18]. Cells were maintained in DMEM/F12 supplemented with 10% FBS, penicillin-streptomycin (100 U/mL), amphotericin B (2.5 µg/mL; MilliporeSigma, A2942), and gentamicin (4 µg/mL; Gibco, 15750060) at 37°C in 5% CO_2.

Doxorubicin treatment and oxygen conditions

Enrichment of the cultures for senescent cells utilized OA chondrocytes treated with doxorubicin to induce DNA damage. Experimental schematics for the doxorubicin treatment protocols are provided in Figs. 1a and 2a. To examine the effects of oxygen tension, chondrocytes were cultured under either 3% O_2, representing physiological oxygen conditions in cartilage, or 21% O_2, representing conventional cell culture conditions and referred to as hyperoxia throughout this study. Both conditions were maintained at 37°C and 5% CO_2. Following 5 days of primary culture, chondrocytes were passaged once (P1) using 0.25% trypsin/EDTA (Fisher Scientific, 25-200-056) and seeded at the desired density in the appropriate culture vessels.

Doxorubicin (Cell Signaling Technology, 5927) was administered at 1 µM under hyperoxia (21% O_2) and 0.5 µM under normoxia (3% O_2). The lower dose for normoxic conditions was necessary since pilot experiments revealed significant cell death using the 1 µM dose. DMSO was used as the vehicle control for all doxorubicin treatments at the corresponding concentrations. Treatments were administered every other day for a

total of 8 days. On the final day, cells underwent a serum-free conditioning period prior to experimental collection. Conditioned media and cellular RNA were collected for downstream proteomic and RNA-sequencing analyses, respectively, while parallel wells were fixed for immunofluorescence or processed for SA-β-gal staining.

RNA isolation and quantitative polymerase chain reaction (qPCR)

RNA was isolated from monolayer adherent cultured chondrocytes using the RNeasy Mini Kit (Qiagen, 74106). The RNA was reverse transcribed into complementary cDNA using the iScript Reverse Transcription Supermix (Bio-Rad, 1708841) and analyzed via quantitative PCR (qPCR) using the iTaq Universal SYBR Green Supermix (Bio-Rad, 1725121). Gene expression was analyzed by normalizing all target genes to the housekeeping gene *GAPDH* using the delta-delta Ct method. The full list of primer sequences is provided in Supplementary Table 2.

RNA-seq processing and quality control

Isolated RNA was used to generate libraries for RNAseq as previously described [19]. The RNA-seq libraries averaged approximately 47.8 million paired-end (2 x 150 bp) reads per sample. Low-quality bases and adapter sequences were trimmed with TrimGalore(v0.6.7), and read quality before and after trimming was assessed with FastQC(v0.12.1) and summarized across samples with MultiQC(v.1.28), retaining 99.2% of read pairs. Trimmed reads were aligned to the GRCh38 primary assembly with STAR (v2.7.11b), derived from the GENCODE release 49 annotation, and on average 84.0% of reads mapped uniquely to the genome. Alignment quality was assessed with Qualimap (v2.3). Reads were average of 93.9% were exonic with a mean 5'-3' coverage

bias ratio of 1.21. Gene expression was quantified with Salmon (v1.10.3) with the GENCODE v49 index (GRCh38.p14), with automatic library-type detection (-l A) and sequence and GC bias correction (--seqBias and --gcBias). Transcript-level estimates with tximeta and collapsed to gene-level counts with summarizeToGene.

Differential RNA-seq analysis

Gene-level counts from tximeta were analyzed with DESeq2 in R (v4.5.0). Doxorubicin-stimulated and DMSO (control) samples were compared separately within each oxygen environment using the design ~ Donor + Treatment, with donor included as a blocking factor because each donor contributed samples to every condition and treatment. Genes with low detection were omitted by requiring at least 10 counts in at least 40% of samples. Shrunken log2 fold change values were calculated using the apeglm method of lfcShrink, and genes with a Benjamini-Hochberg adjusted p-value < 0.05 and an absolute shrunken log2 fold change > 1 were considered differentially expressed. A full list of the RNA-seq results with log2fc is provided in Supplementary Table 3 and will be deposited in NIH's database of Genotypes and Phenotypes (dbGaP). To examine all samples on a common scale, counts from every sample were combined into a single model with the design ~ Donor + Condition + Treatment + Condition:Treatment. Counts from this model were variance-stabilized (vst) and projected by principal component analysis across all retained genes.

Immunofluorescence

Cells cultured on glass-bottom dishes were fixed with 4% paraformaldehyde at room temperature (RT) for 15 min and washed with 1× PBS. Cells were permeabilized

with 0.5% Triton X-100 in 1× PBS at RT for 10 min, followed by PBS washes. Cells were then blocked with 3% BSA and 0.5% Tween-20 in 1× PBS at RT for 30 min with constant agitation. Following blocking, cells were incubated overnight at 4°C with primary antibodies diluted in 1% BSA and 0.3% Triton X-100: anti-p21/Waf1/Cip1 (1:1000; Cell Signaling Technology, 2947) and CINtec p16 (1:1; Roche, 06695248001). After primary antibody incubation, cells were washed with 1× PBS and incubated for 1 hour at RT with Alexa Fluor 555 donkey anti-rabbit (RFP) and Alexa Fluor 647 chicken anti-mouse (Cy5) secondary antibodies, each diluted 1:500. Cells were subsequently washed with 1X PBS and counterstained with DAPI (1:1000) for 5 min at RT and imaged using an EVOS FL fluorescence imaging system. Secondary antibody-only controls without primary antibodies were included to assess nonspecific binding of the secondary antibody (not shown). Minimal to no background fluorescence was observed under the imaging conditions used. CellProfiler software was used to quantify fluorescence.

Machine Learning Models

The RNA-seq data were applied to the machine learning models SenCID, DeepScence, and the human universal senescence index (hUSI) to generate senescence scores and predictions. All models were implemented and executed in Python using the Anaconda platform. For each model, an individual folder and an Anaconda environment were created. The documentation provided in the GitHub repositories for each of the models was followed. Preprocessing steps included retrieving source code and scripts from the GitHub repositories, installing all necessary R and Python packages, and appropriately formatting each dataset for input. All bulk

RNA-sequencing data was formatted in Microsoft Excel and exported as a tab-delimited text file for input into each machine learning model. To satisfy the model input requirements, each participant was represented as a single observation and stored in individual columns, while each gene was represented as a row. The hyperoxia and normoxia datasets were processed and analyzed independently. After model execution, the individual contributions of each gene and scoring results from each model were retrieved for further analysis. Additional details are provided in the Supplementary Methods.

GDF-15 chondrocyte treatments and RNA-seq analysis

We used four normal human chondrocyte donors for treatment with recombinant human GDF-15 (Thermo Fisher Scientific, 120-28C). Freshly isolated cells were plated in monolayer culture in DMEM with 10% FBS. After 2–3 days the medium was changed to 1% FBS and cells were treated with either 1 ng/mL or 10 ng/mL GDF-15 or PBS as a control for 6 or 18 h. Following treatment, RNA was collected using DNA/RNA Shield (Zymo Research, R1100-50) according to the manufacturer's instructions and submitted to Plasmidsaurus (Louisville, KY) for RNA sequencing. The Plasmidsaurus RNA-Seq service uses 3′-end counting on the Illumina platform. Differential gene expression and enrichment analyses were performed using the Plasmidsaurus analysis pipeline (detailed in supplementary methods). Differentially expressed genes, enrichment, and raw gene count files were obtained for further analysis. All data visualization and statistical analyses were performed using R and GraphPad Prism.

Proteomics Analysis

Serum-free conditioned media samples were collected from chondrocytes following senescence stimulation (Figure 2a). Conditioned media samples were precipitated with cold acetone containing 10% trichloroacetic acid (TCA) and incubated at −20°C overnight. Following centrifugation, protein pellets were resuspended in 50 mM ammonium bicarbonate and digested overnight with trypsin/Lys-C at 37°C. The reaction was quenched by adding 1% formic acid, and resulting peptides were purified using C18 stage tips. Peptides were prepared with 1% formic acid for LC-MS/MS analysis. Samples were analyzed on an LC-MS/MS system consisting of an Orbitrap Eclipse Mass Spectrometer and a Vanquish Neo nano-UPLC system (Thermo Scientific, Waltham, MA). The peptide mixture was injected via a trap-and-elute procedure using a Thermo Scientific Acclaim PepMap 100 trap column (cat# 164946) and a Thermo Scientific DNV PepMap Neo (cat# DNV75500PN) analytical column. Peptides were separated employing linear gradient elution consisting of water (A) and 80% acetonitrile (B), both of which contained 0.1% formic acid. Data was collected by data-independent acquisition (DIA), in which fragmentation occurs in 44 static DIA windows, each 10Th wide, over 500-900 m/z. Cycle time was set to 3 seconds between adjacent survey spectra. To identify proteins, spectra were searched against the UniProt human protein FASTA database (20,395 annotated entries, Jun 2021) using the Pulsar search engine within Spectronaut v20 (Biognosys AG, Switzerland). Search parameters were as follows: FT-trap instrument; parent mass error tolerance, 10 ppm; fragment mass error tolerance, 0.6 Da (monoisotopic); enzyme, Pepsin (full); # maximum missed cleavages, 2; variable modifications, +15.995 Da (oxidation) on methionine.

MetaboAnalyst was used to analyze and process proteomic abundance data from hyperoxia and normoxia datasets. Analysis included omitting proteins present in less than 50% of all samples, and non-detected values were imputed with 1/5 of the lowest detected sample (Fig. S4a). For protein abundance normalization, each protein's LC-MS abundance was divided by the donor's total cell count. Fig. S2a-b show final cell counts post-treatment, and Supplementary Table 6 provides a full list of log2 fold-change comparisons to the DMSO control. Normalized protein abundance was calculated as follows:

$$Normalized\ Protein\ abundance = \frac{Doxorubicin\ treated\ donor\ protein}{Cell\ count\ post\ treatment}$$

Statistical Analysis

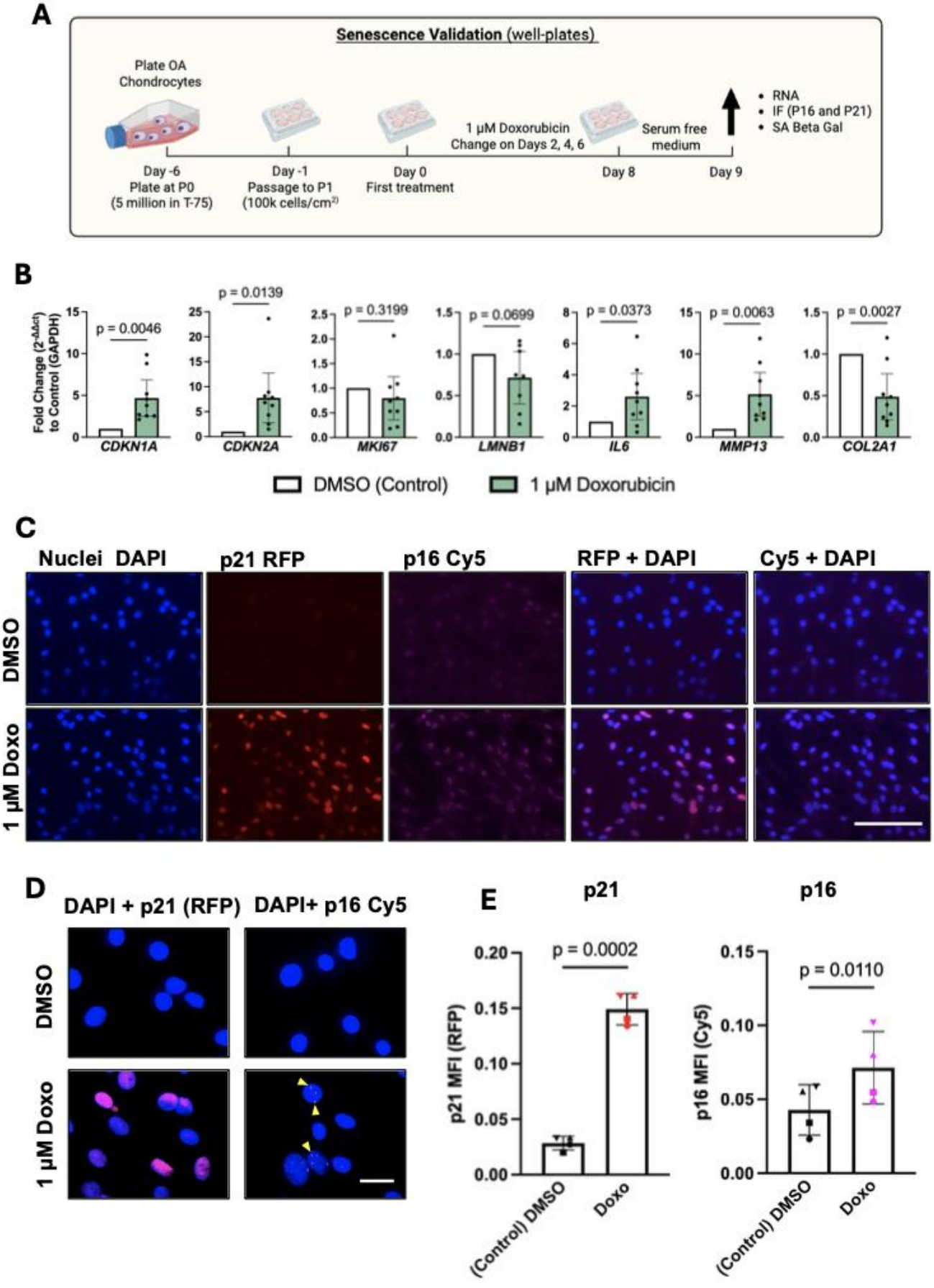
GraphPad Prism was used for statistics. All bar graphs and grouped dot plots with individual data points are shown as mean with standard deviation. T-tests were used for paired comparisons that followed normal distributions. For data that did not meet normal distribution, a Wilcoxon signed-rank test was applied. One-sample t-tests were used to determine whether qPCR sample means differed significantly from no change (fold change of 1).

Results

Doxorubicin induces classical senescence markers in OA chondrocytes

To determine the ability of doxorubicin to enrich OA chondrocyte cultures for senescent cells, we treated cells with 1μM of doxorubicin in the standard tissue culture oxygen environment (21% O_2) over a 9-day period to allow for stable senescence

induction (Fig. 1A). These conditions resulted in a significant increase in the expression of the senescence markers *CDKN1A* (p21) and *CDKN2A* (p16), along with a significant increase in SASP factors *IL6* and *MMP13* (Fig.1B). Although not statistically significant due to low levels under control conditions, the proliferation marker *MKI67* and senescence marker *LMNB1* showed decreased expression, consistent with senescence. The matrix gene *COL2A1* was also downregulated (Fig. 1B). Immunofluorescence staining showed increased p21 and p16 in response to doxorubicin in chondrocytes from each of 4 individual donors (Fig. 1C-E and supplemental Fig. S1C-D). Staining for p21 was primarily found in the nucleus, while p16 was also noted in the cytosol. Microscopy images of cells post-treatment showed an elongated phenotype resembling a spindle-like morphology (Fig. S1A). SA-β-gal staining showed some positive cells in the DMSO controls, which significantly increased in 2 of the 3 donors treated with doxorubicin (Fig. S1B). Together, these results demonstrate senescence enrichment in OA chondrocyte cultures treated with doxorubicin for 8 days using standard markers.

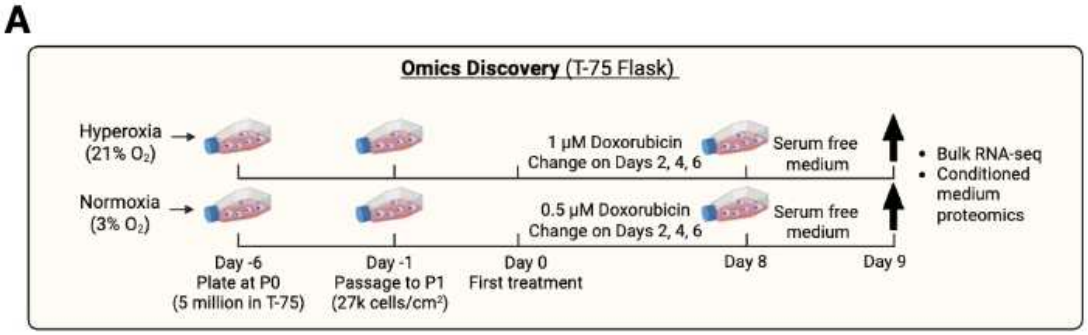

A
Senescence Validation (well-plates)
Plate OA Chondrocytes
Day -6 Plate at P0 (5 million in T-75)
Day -1 Passage to P1 (100k cells/cm2)
Day 0 First treatment
1 µM Doxorubicin Change on Days 2, 4, 6
Day 8
Serum free medium
Day 9
RNA
IF (P16 and P21)
SA Beta Gal
B
Fold Change (2-ΔΔct) to Control (GAPDH)
p = 0.0046
p = 0.0139
p = 0.3199
p = 0.0699
p = 0.0373
p = 0.0063
p = 0.0027
CDKN1A
CDKN2A
MKI67
LMNB1
IL6
MMP13
COL2A1
DMSO (Control)
1 µM Doxorubicin
C
Nuclei DAPI
p21 RFP
p16 Cy5
RFP + DAPI
Cy5 + DAPI
DMSO
1 µM Doxo
D
DAPI + p21 (RFP)
DAPI+ p16 Cy5
DMSO
1 µM Doxo
E
p21
p16
p = 0.0002
p = 0.0110
p21 MFI (RFP)
p16 MFI (Cy5)
(Control) DMSO
Doxo

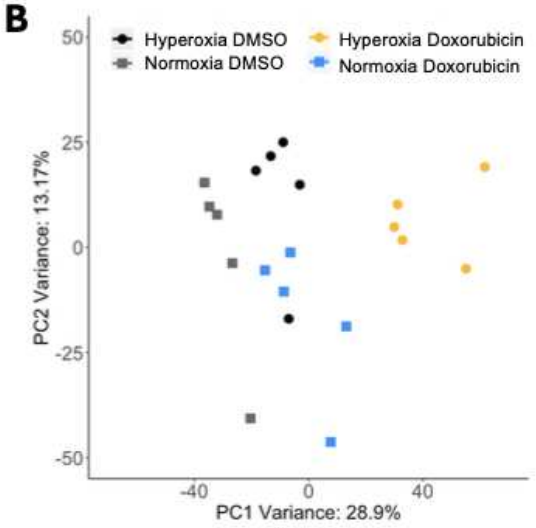
Effects of doxorubicin and oxygen concentration on chondrocyte gene expression

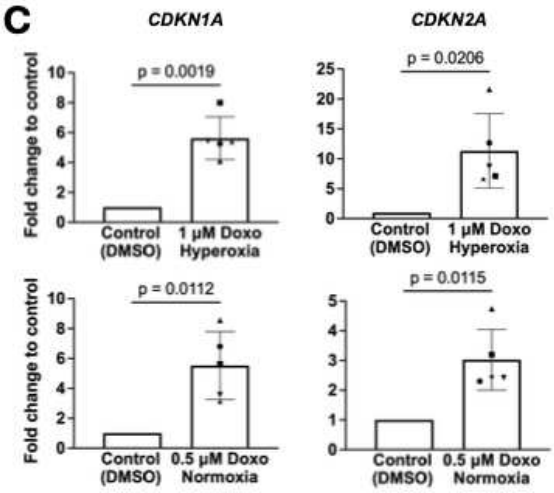
We next used doxorubicin to increase the proportion of senescent cells within the cultures under physiologic oxygen conditions (3% oxygen), which we refer to as normoxia, compared to a traditional incubator environment (21% oxygen), which we refer to as hyperoxia. Cells isolated from five OA donors were used for treatments, followed by the collection of RNA for gene expression analysis using bulk RNA-seq and serum-free conditioned medium for proteomics analysis by mass spectrometry (Fig. 2A). Preliminary experiments utilizing 1μM doxorubicin in normoxic conditions noted significant cell death and therefore the dose was reduced to 0.5 μM to promote higher viability. Under these conditions cell counts were relatively stable across control and doxorubicin conditions (Fig. S2A-B).

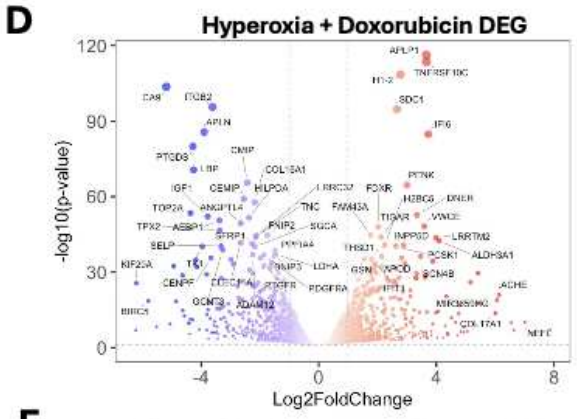
Principal component analysis showed clustering based on doxorubicin treatment, oxygen environment, and their interaction (Fig. 2B). To provide an initial validation of senescence induction in these samples, CDKN1A, and CDKN2A expression were analyzed by qPCR and this revealed significant upregulation of both markers in doxorubicin-treated samples compared to controls under both oxygen conditions (Fig. 2C). Volcano plots of RNAseq data for both hyperoxia (Fig. 2D) and normoxia (Fig. 2E) conditions showed significant upregulation of *TNFRSF10C*, *APOD*, *H1-2*, *PENK*, and *PCSK1,* and significant downregulation of *KIF20A*, *TOP2A*, *TK1*, *TPX2,* and *ITGB2* across both oxygen conditions. Significantly upregulated genes unique to hyperoxia were *VWECE* and *IFI6*, and unique to normoxia were *PAPPA* and *SYT12*.

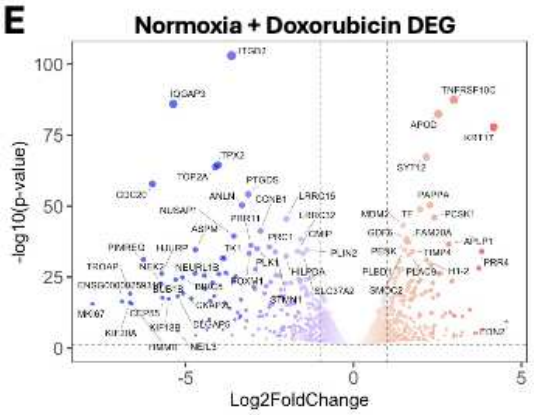
Hallmarks analysis identified several pathways upregulated by doxorubicin under both oxygen conditions, including the p53 pathway, DNA repair, peroxisome, and oxidative phosphorylation (Fig. 2F-G). In contrast, G2/M checkpoint, hypoxia, E2F targets, and mitotic spindle were downregulated under both conditions. (Fig. 2F-G). Similar enrichment patterns were observed under both oxygen conditions across the Hallmark, GO biological process (GO-BP), and KEGG analyses (Fig. S2). Reactome analysis showed increased defective pyroptosis, PRC2 methylation of histones and DNA, and decreased mitotic spindle checkpoint. The senescence-associated secretory phenotype (SASP) was uniquely upregulated under hyperoxia (Fig. S2C-D). GO-BP identified upregulation of heparan sulfate proteoglycan metabolic processes and downregulation of metaphase plate congression (Fig. S2E-F), while KEGG analysis showed enrichment of systemic lupus erythematosus and decreased cell cycle pathways (Fig. S2G-H).

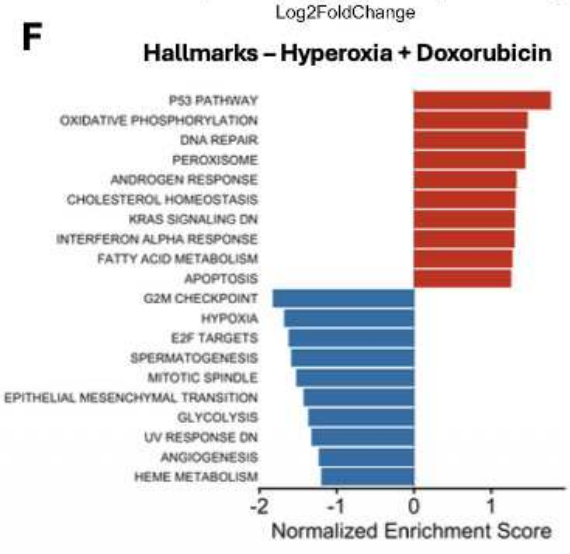

A
Omics Discovery (T-75 Flask)
Hyperoxia (21% O2)
Normoxia (3% O2)
1 µM Doxorubicin Change on Days 2, 4, 6
0.5 µM Doxorubicin Change on Days 2, 4, 6
Serum free medium
Serum free medium
• Bulk RNA-seq
• Conditioned medium proteomics
Day -6 Plate at P0 (5 million in T-75)
Day -1 Passage to P1 (27k cells/cm²)
Day 0 First treatment
Day 8
Day 9

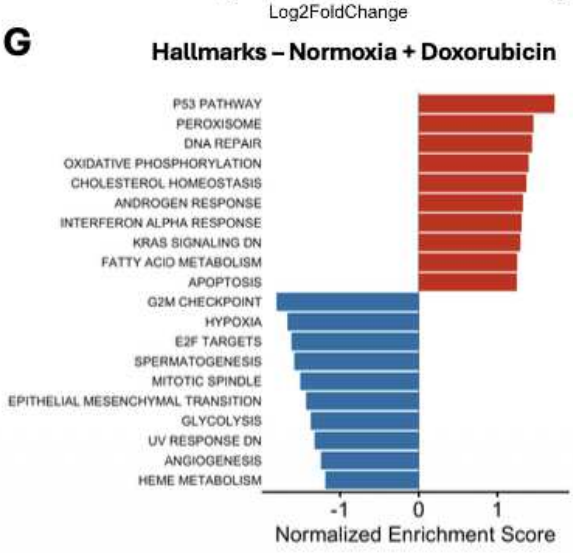

B
Hyperoxia DMSO
Hyperoxia Doxorubicin
Normoxia DMSO
Normoxia Doxorubicin
PC2 Variance: 13.17%
PC1 Variance: 28.9%


C
CDKN1A
CDKN2A
p = 0.0019
p = 0.0206
p = 0.0112
p = 0.0115
Fold change to control
Control (DMSO)
1 µM Doxo Hyperoxia
0.5 µM Doxo Normoxia


D
Hyperoxia + Doxorubicin DEG
-log10(p-value)
Log2FoldChange


E
Normoxia + Doxorubicin DEG
-log10(p-value)
Log2FoldChange


F
Hallmarks – Hyperoxia + Doxorubicin
P53 PATHWAY
OXIDATIVE PHOSPHORYLATION
DNA REPAIR
PEROXISOME
ANDROGEN RESPONSE
CHOLESTEROL HOMEOSTASIS
KRAS SIGNALING DN
INTERFERON ALPHA RESPONSE
FATTY ACID METABOLISM
APOPTOSIS
G2M CHECKPOINT
HYPOXIA
E2F TARGETS
SPERMATOGENESIS
MITOTIC SPINDLE
EPITHELIAL MESENCHYMAL TRANSITION
GLYCOLYSIS
UV RESPONSE DN
ANGIOGENESIS
HEME METABOLISM
Normalized Enrichment Score


G
Hallmarks – Normoxia + Doxorubicin
P53 PATHWAY
PEROXISOME
DNA REPAIR
OXIDATIVE PHOSPHORYLATION
CHOLESTEROL HOMEOSTASIS
ANDROGEN RESPONSE
INTERFERON ALPHA RESPONSE
KRAS SIGNALING DN
FATTY ACID METABOLISM
APOPTOSIS
G2M CHECKPOINT
HYPOXIA
E2F TARGETS
SPERMATOGENESIS
MITOTIC SPINDLE
EPITHELIAL MESENCHYMAL TRANSITION
GLYCOLYSIS
UV RESPONSE DN
ANGIOGENESIS
HEME METABOLISM
Normalized Enrichment Score

Effects of doxorubicin and oxygen concentration on senescence scores

To further evaluate the senescent state of the cells, we used senescence-related gene sets and computational programs to generate senescence scores for comparison across culture conditions and cell types. We used SenCID, hUSI, and DeepScence[14–16] to score senescence in our RNA-seq data (Fig. 3A). SenCID was developed using machine learning trained on publicly available senescence transcriptome datasets across 30 different cell types to identify distinct senescence-associated transcriptional identities. SenCID has 6 total categories that relate to different senescence programs and different cell types. The SID3 category demonstrated a clear separation of doxorubicin-treated cells from controls under both oxygen conditions that passed the threshold line of 0.5 (Fig. 3B). This finding was consistent with the SID3 categorization of senescent osteoarthritic chondrocytes that was reported by the authors of the SenCID program[14]. Plotted individual donors revealed a significant increase in SID3 scores with doxorubicin treatment under both oxygen conditions (Fig. 3D).

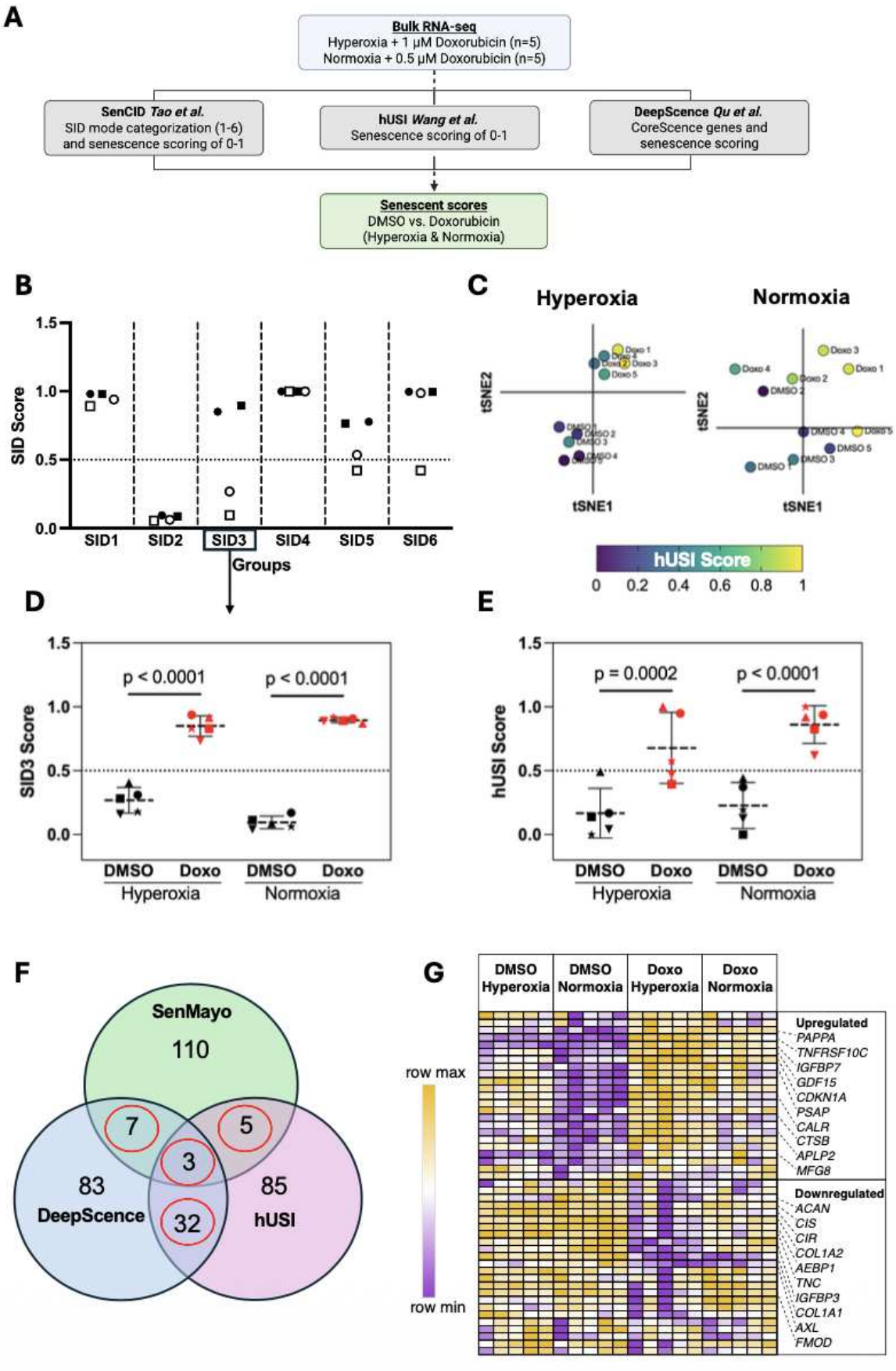
hUSI was developed by integrating publicly available senescence-associated RNA-seq datasets and applying a One-Class Logistic Regression (OCLR) model to derive a universal senescence signature. For the hUSI analysis, donor distribution was examined in t-SNE plots, where a clear separation between controls and the doxorubicin treatments was observed, specifically in the hyperoxia condition (Fig. 3C). All doxorubicin treated samples demonstrated an overall higher hUSI score compared to controls under both oxygen tensions (Fig. 3E). hUSI scores from individual donors at both oxygen tensions showed a significant increase in doxorubicin-treated cells under both conditions; normoxia showed a clear separation across the senescence threshold

for all donors, whereas in hyperoxia, two doxorubicin-treated samples fell just below the senescence threshold.

We next used Deepscence[16], which uses a robust senescence gene set of 39 genes (CoreScence genes) developed from deep neural network analysis of single-cell and spatial transcriptomic data across multiple tissues, and noted bimodal score distributions under both normoxia and hyperoxia. This distribution indicates a separation of the doxorubicin-treated cells from controls, with hyperoxia showing a more pronounced separation between the two Gaussian components (Fig. S3B-C). To further evaluate how the CoreScence set of 39 genes was represented in our bulk RNA-seq data, we mapped the CoreScence genes onto the ranked lists of differentially expressed genes (DEGs) for each condition. In hyperoxia, the majority of CoreScence genes were concentrated toward the extremes of the ranked distribution (Fig. S3D). In contrast, under normoxia, a larger proportion of CoreScence genes were closer to the center of the distribution, within the less differentially expressed region, suggesting a more modest senescence-associated transcriptional signal (Fig. S3E). *TNFRS10C* was the most highly regulated CoreScence gene, and *CDK1* was a negatively regulated gene across both datasets. *SERPINE1* in the hyperoxia condition and *PARP1*, *HMGB1,* and *CXCL1* in the normoxia condition showed minimal to no change (Fig. S3D-E).

To further assess the transcriptional senescence signatures identified by the different scoring programs, we compared the ranked genes generated by hUSI and DeepScence with the SenMayo reference list of 125 senescence-associated genes[20]. SenCID was not included in this gene-level comparison because the algorithm categorizes samples into six senescence identification (SID) groups based on distinct

sets of differentially expressed genes, rather than generating a single ranked list of gene contributions. We focused this analysis on the normoxia dataset because this oxygen tension more closely reflects the OA microenvironment, and the modeling results from SenCID, DeepScence, and hUSI showed separation between senescence states. For comparison, the top 125 ranked genes from hUSI and DeepScence were selected to match the size of the SenMayo reference set, and the list of these genes are provided in Supplementary Table 4. Comparison of the three gene sets identified 47 genes shared by two or more groups, with the largest shared set consisting of 32 genes common to the DeepScence and hUSI lists (Fig. 3F). The complete list of shared genes and the corresponding groups in which each gene was identified are provided in Supplementary Table 5. We next examined the expression of these 47 shared genes in the hyperoxia dataset and found that the genes showed both increased and decreased expression following doxorubicin treatment (Fig. 3G). Among the most highly upregulated genes were *TNFRSF10C, GDF15, IGFBP7, CDKN1A,* and *PAPPA*, whereas *ACAN, TNC, COL1A1, COL1A2,* and *IGFBP3* were among the most downregulated genes (Fig. 3G).


A
Bulk RNA-seq
Hyperoxia + 1 µM Doxorubicin (n=5)
Normoxia + 0.5 µM Doxorubicin (n=5)
SenCID Tao et al.
SID mode categorization (1-6) and senescence scoring of 0-1
hUSI Wang et al.
Senescence scoring of 0-1
DeepScence Qu et al.
CoreScence genes and senescence scoring
Senescent scores
DMSO vs. Doxorubicin (Hyperoxia & Normoxia)
B
SID Score
SID1
SID2
SID3
SID4
SID5
SID6
Groups
C
Hyperoxia
Normoxia
tSNE1
tSNE2
hUSI Score
D
SID3 Score
p < 0.0001
p < 0.0001
DMSO
Doxo
Hyperoxia
Normoxia
E
hUSI Score
p = 0.0002
p < 0.0001
F
SenMayo
110
83
DeepScence
85
hUSI
7
5
3
32
G
DMSO Hyperoxia
DMSO Normoxia
Doxo Hyperoxia
Doxo Normoxia
row max
row min
Upregulated
PAPPA
TNFRSF10C
IGFBP7
GDF15
CDKN1A
PSAP
CALR
CTSB
APLP2
MFG8
Downregulated
ACAN
CIS
CIR
COL1A2
AEBP1
TNC
IGFBP3
COL1A1
AXL
FMOD

The effects of chondrocyte senescence induction on the secretome

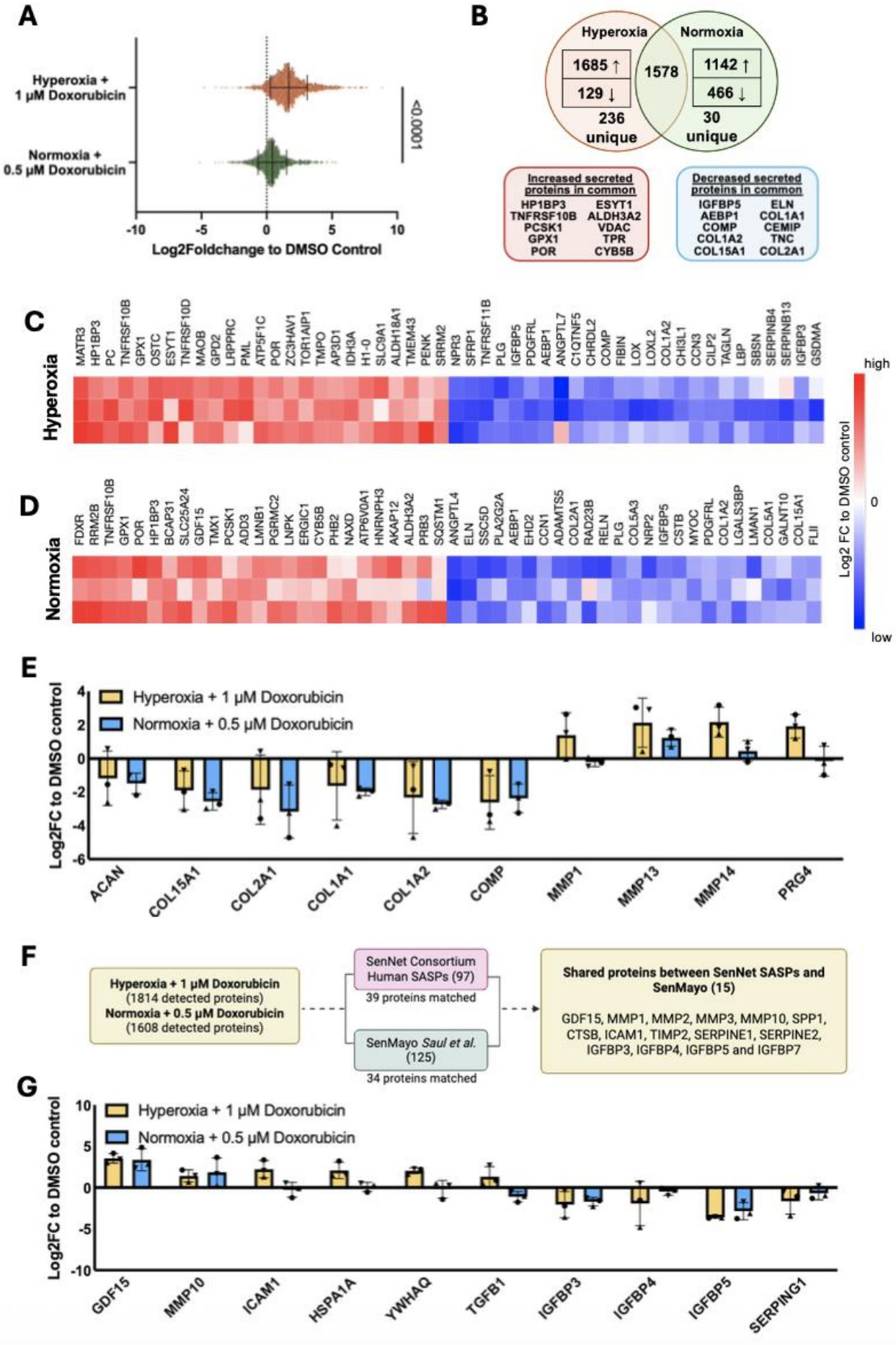
Serum-free conditioned media was collected from the same cultures used for RNAseq analysis and proteomics analysis was performed using mass spectrometry. The PCA plot for hyperoxia showed two separate clusters for control and doxorubicin-treated cells (Fig. S4B). The PCA plot for normoxia showed greater dispersion among control samples, whereas doxorubicin-treated samples formed a tighter cluster that fell within the control sample distribution (Fig. S4B-C). Two donors were omitted from further analysis due to low protein abundance (Fig. S4B-C). Differential protein analysis demonstrated a shift towards a more secretory phenotype induced by doxorubicin treatments that was more prominent under hyperoxic conditions (Fig. 4A). Compared to controls, doxorubicin under hyperoxia increased secretion of 1685 proteins while 129 decreased, whereas doxorubicin under normoxia increased secretion of 1142 proteins while 466 decreased (Fig. 4B). The hyperoxia condition showed 236 uniquely identified secreted proteins while the normoxia condition showed 30 proteins. Common proteins that were increasingly secreted were HP1BP3, TNFRSF10B, PCSK1, and GPX1, while common proteins that were decreasingly secreted included IGFBP5, AEBP1, COMP, COL2A1, and ELN.

A total of 1578 proteins were common between the datasets when including those that showed increased or decreased abundance with doxorubicin treatment compared to control under either oxygen condition. Over half of the proteins present in both datasets were classified by Ingenuity Pathway Analysis (IPA) as cytoplasmic, followed by equal proportions of plasma membrane, nuclear, and extracellular space proteins (Fig. S4B-C). We compiled heatmaps of the most abundant proteins that

increased or decreased with doxorubicin treatment compared to controls for both hyperoxia (Fig. 4C) and normoxia (Fig. 4D) conditions. The top 5 highest in hyperoxia were MATR3, HP1BP3, PC, TNFRSF10B, and GPX1 while those that decreased included NPR3, SFRP1, TNFRSF 11B, PLG, and IGFBP5 (Fig. 4D). The top 5 highest in normoxia were FXDR, RRM2B, TNFRSF10B, GPX1, and POR and those that decreased included ANGPTL4, ELN, SSC5D, PLA2G2A, and AEBP1 (Fig. 4D). Only TNFRSF10B was among the top 5 hits in both oxygen conditions. We also searched the results for key cartilage matrix proteins, including collagens, aggrecan, COMP, and PRG4, as well as the matrix metalloproteinases MMP1, 13, and 14. We observed consistent decreases in secretion of the extracellular matrix proteins after senescence enrichment with doxorubicin under both oxygen conditions, except for PRG4, which was increased under hyperoxia only (Fig. 4E). Hyperoxia also increased secretion of MMP1, 13, and 14, while normoxia only increased MMP13.

To determine whether the secreted proteins identified in our datasets have been previously characterized as senescence-associated or SASP proteins in other cell types, we focused on the SenNet human SASP (Supplementary Table 7) selected from the larger SenNet gene list, and SenMayo[20] protein lists and matched them to proteins detected under hyperoxic and normoxic conditions. We identified 39 SenNet SASP proteins and 34 SenMayo proteins that were present in our datasets (Supplementary Tables 8 and 9). Among these, 15 proteins were shared between the SenNet SASP and SenMayo lists, including GDF15, ICAM1, MMP1, MMP2, MMP3, MMP10, IGFBP3, IGFBP5, IGFBP7, SPP1, SERPINE1, SERPINE2, CTSB, TIMP1, and TIMP2 (Figure 4F). Of these shared proteins, GDF15 showed the highest secretion

under both oxygen conditions (Fig. 4G). MMP1, MMP3, and MMP10 were the matrix-degrading enzymes that showed the greatest differential regulation. Several proteins displayed oxygen-dependent changes in secretion, with ICAM1, HSPA1A, YWHAQ, and TGFB1 increased under hyperoxia but unchanged or modestly decreased under normoxia. In contrast, IGFBP3, IGFBP4, IGFBP5, and SERPING1 were consistently decreased under both conditions. Other shared SASP proteins, including MMP2, SPP1, CTSB, TIMP2, SERPINE1, SERPINE2, and IGFBP7, showed no change in secretion relative to control (not shown).


A
Hyperoxia + 1 µM Doxorubicin
Normoxia + 0.5 µM Doxorubicin
<0.0001
-10
-5
0
5
10
Log2Foldchange to DMSO Control
B
Hyperoxia
Normoxia
1685 ↑
129 ↓
1578
1142 ↑
466 ↓
236 unique
30 unique
Increased secreted proteins in common
HP1BP3 ESYT1
TNFRSF10B ALDH3A2
PCSK1 VDAC
GPX1 TPR
POR CYB5B
Decreased secreted proteins in common
IGFBP5 ELN
AEBP1 COL1A1
COMP CEMIP
COL1A2 TNC
COL15A1 COL2A1
C
Hyperoxia
MATR3 HP1BP3 PC TNFRSF10B GPX1 OSTC ESYT1 TNFRSF10D MAOB GPD2 LRPPRC PML ATP5F1C POR ZC3HAV1 TOR1AIP1 TMPO AP3D1 IDH3A H1-0 SLC9A1 ALDH18A1 TMEM43 PENK SRRM2 NPR3 SFRP1 TNFRSF11B PLG IGFBP5 PDGFRL AEBP1 ANGPTL7 C1QTNF5 CHRDL2 COMP FIBIN LOX LOXL2 COL1A2 CHI3L1 CCN3 CILP2 TAGLN LBP SBSN SERPINB4 SERPINB13 IGFBP3 GSDMA
high
Log2 FC to DMSO control
0
low
D
Normoxia
FDXR RRM2B TNFRSF10B GPX1 POR HP1BP3 BCAP31 SLC25A24 GDF15 TMX1 PCSK1 ADD3 LMNB1 PGRMC2 LNPK ERGIC1 CYB5B PHB2 NAXD ATP6V0A1 HNRNPH3 AKAP12 ALDH3A2 PRB3 SQSTM1 ANGPTL4 ELN SSC5D PLA2G2A AEBP1 EHD2 CCN1 ADAMTS5 COL2A1 RAD23B RELN PLG COL5A3 NRP2 IGFBP5 CSTB MYOC PDGFRL COL1A2 LGALS3BP LMAN1 COL5A1 GALNT10 COL15A1 FLI
E
Log2FC to DMSO control
Hyperoxia + 1 µM Doxorubicin
Normoxia + 0.5 µM Doxorubicin
4
2
0
-2
-4
-6
ACAN
COL15A1
COL2A1
COL1A1
COL1A2
COMP
MMP1
MMP13
MMP14
PRG4
F
Hyperoxia + 1 µM Doxorubicin
(1814 detected proteins)
Normoxia + 0.5 µM Doxorubicin
(1608 detected proteins)
SenNet Consortium Human SASPs (97)
39 proteins matched
SenMayo Saul et al. (125)
34 proteins matched
Shared proteins between SenNet SASPs and SenMayo (15)
GDF15, MMP1, MMP2, MMP3, MMP10, SPP1, CTSB, ICAM1, TIMP2, SERPINE1, SERPINE2, IGFBP3, IGFBP4, IGFBP5 and IGFBP7
G
Log2FC to DMSO control
Hyperoxia + 1 µM Doxorubicin
Normoxia + 0.5 µM Doxorubicin
10
5
0
-5
-10
GDF15
MMP10
ICAM1
HSPA1A
YWHAQ
TGFB1
IGFBP3
IGFBP4
IGFBP5
SERPING1

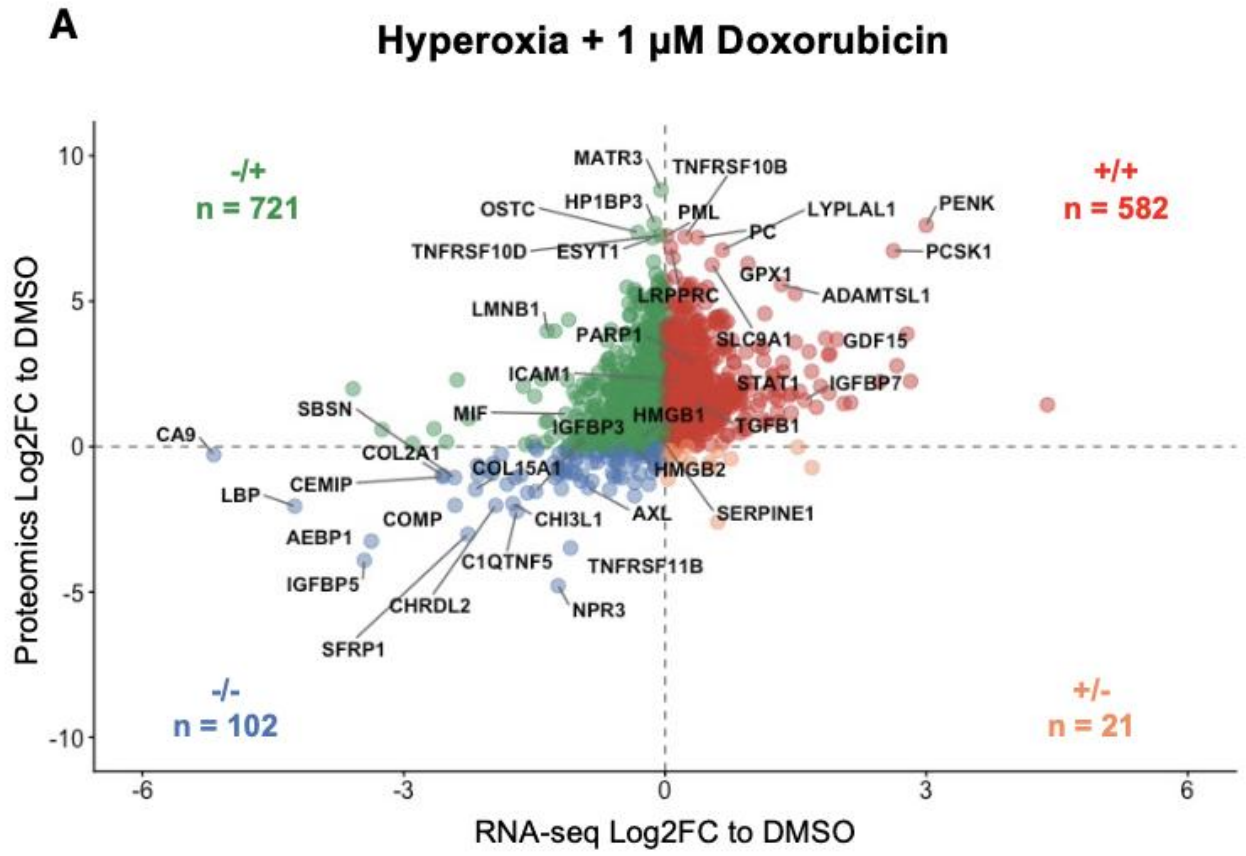
SASP factors expressed and secreted by human OA chondrocytes in response to senescence enrichment

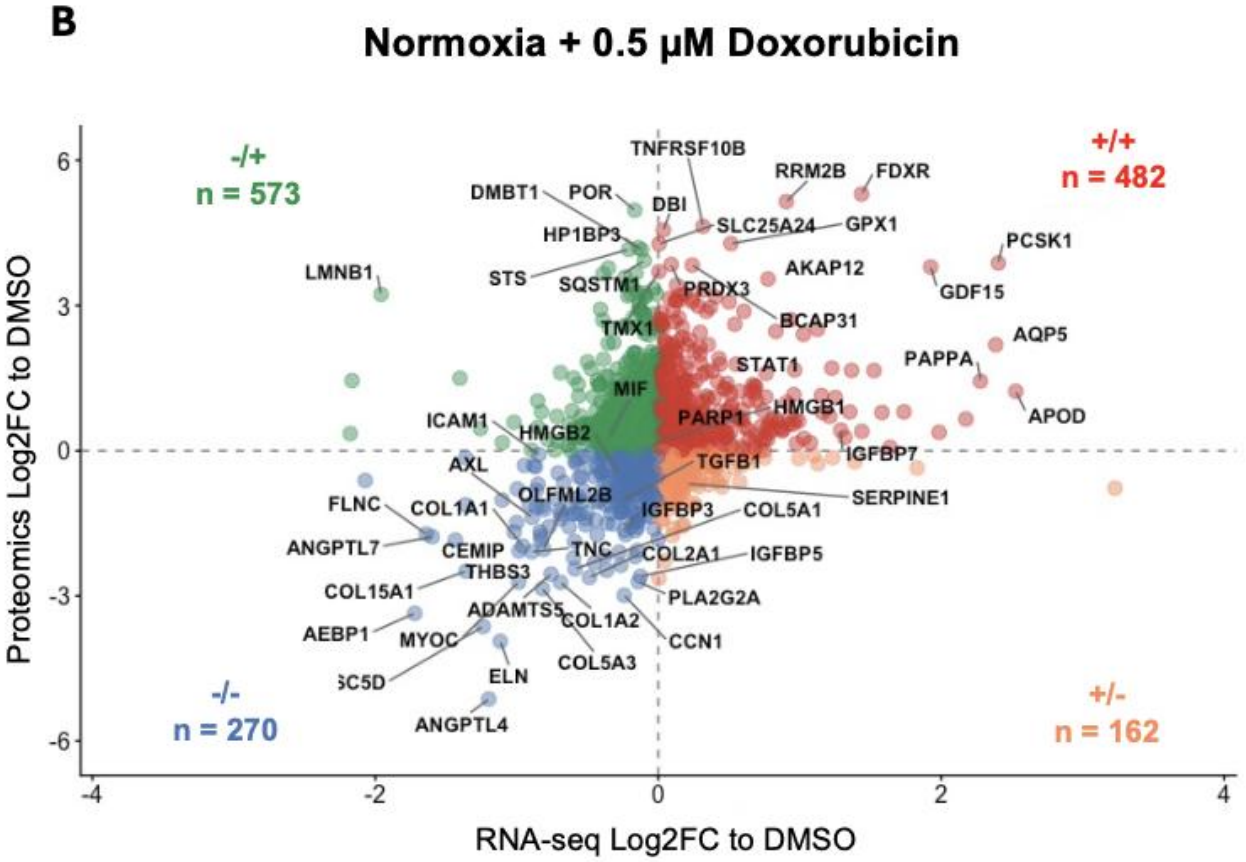
To identify SASP factors regulated at both the transcriptional and protein-secretion levels, we integrated our bulk RNA-seq and proteomics datasets to identify proteins that showed gene expression changes and secretion changes with doxorubicin treatment. A total of 1696 proteins were matched in the hyperoxia RNA-seq and proteomics datasets, with 582 proteins upregulated and 102 proteins downregulated at both the secretion and transcriptional levels (Fig. 5A). We also found 721 proteins upregulated in secretion but transcriptionally downregulated and 21 proteins were downregulated in secretion but transcriptionally upregulated, indicating a discordance between gene expression and protein secretion. In the normoxia RNA-seq and proteomics datasets, we found 1467 matches with 482 upregulated and 270 downregulated at the secretion and transcriptional level (Fig. 5B). Of these, 573 proteins showed increased secretion but were transcriptionally downregulated, and 162 showed decreased secretion but were transcriptionally upregulated. H1BP3 was highly secreted with minimal changes in gene expression in both oxygen conditions. LMNB1, a gene that encodes the nuclear protein lamin B1, was transcriptionally downregulated but highly secreted in both datasets. Loss of lamin B1 from the nucleus is a well-described marker of cellular senescence[21,22].

GDF15, a well-established Corescence gene and SASP protein, was highly upregulated with senescence enrichment at both oxygen concentrations in the RNAseq and proteomic datasets. To confirm the proteomics result, we measured GDF15

521 secretion by ELISA and found higher levels under hyperoxia (Fig. 5A). Similarly, the

522 RNA-seq data showed higher GDF15 expression under hyperoxia (Fig. 5B).

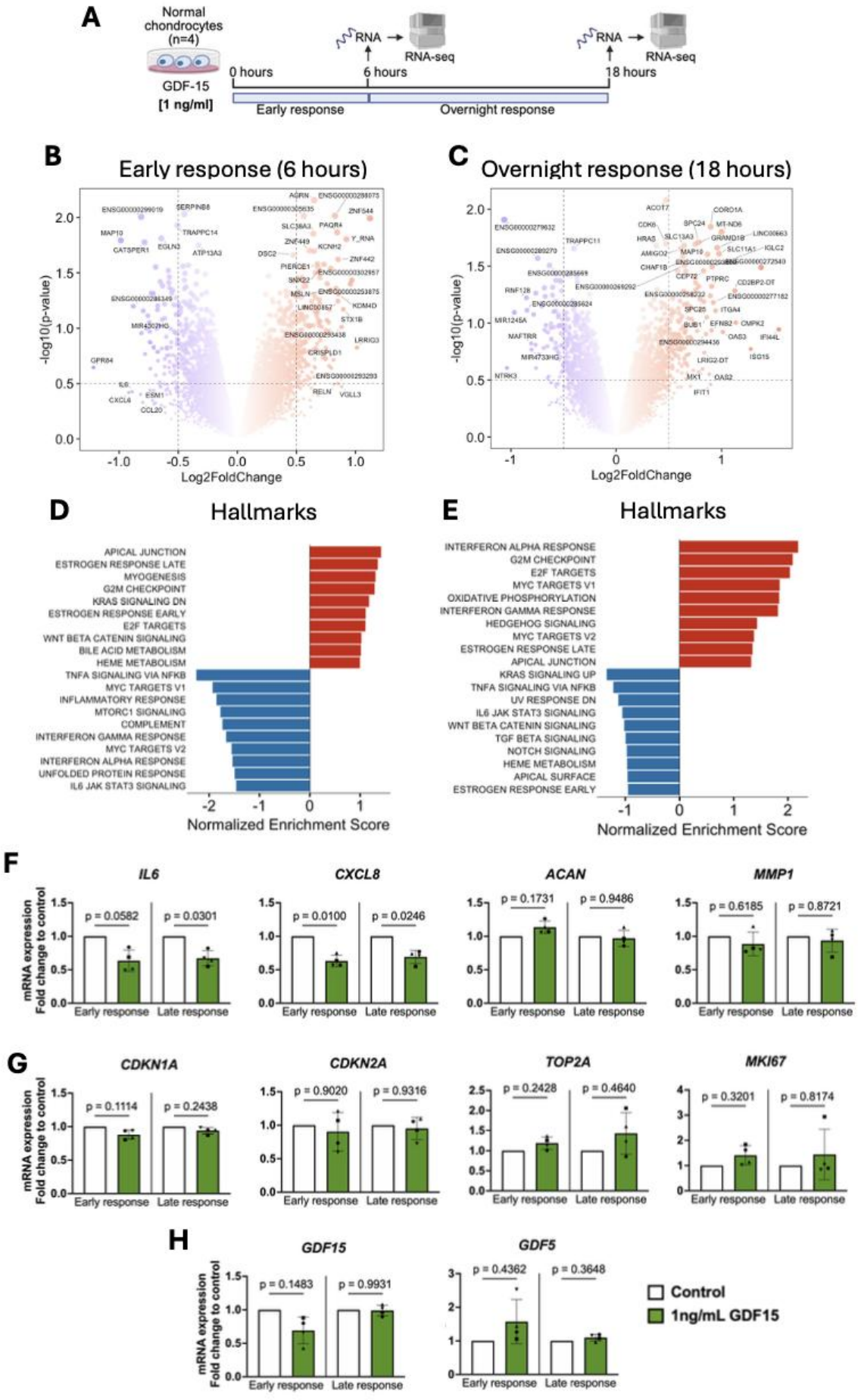

A
Hyperoxia + 1 µM Doxorubicin
-/+
n = 721
+/+
n = 582
-/-
n = 102
+/-
n = 21
MATR3
TNFRSF10B
OSTC
HP1BP3
PML
LYPLAL1
PENK
PC
TNFRSF10D
ESYT1
PCSK1
GPX1
ADAMTSL1
LRPPRC
LMNB1
PARP1
SLC9A1
GDF15
ICAM1
STAT1
IGFBP7
SBSN
MIF
HMGB1
IGFBP3
TGFB1
CA9
COL2A1
COL15A1
HMGB2
LBP
CEMIP
AXL
SERPINE1
COMP
CHI3L1
AEBP1
C1QTNF5
TNFRSF11B
IGFBP5
CHRDL2
NPR3
SFRP1
Proteomics Log2FC to DMSO
RNA-seq Log2FC to DMSO
10
5
0
-5
-10
-6
-3
0
3
6


B
Normoxia + 0.5 µM Doxorubicin
-/+
n = 573
+/+
n = 482
-/-
n = 270
+/-
n = 162
TNFRSF10B
RRM2B
FDXR
DMBT1
POR
DBI
SLC25A24
GPX1
HP1BP3
PCSK1
LMNB1
STS
SQSTM1
AKAP12
PRDX3
GDF15
BCAP31
TMX1
AQP5
STAT1
PAPPA
MIF
ICAM1
PARP1
HMGB1
APOD
HMGB2
IGFBP7
AXL
TGFB1
OLFML2B
SERPINE1
FLNC
COL1A1
IGFBP3
COL5A1
ANGPTL7
CEMIP
TNC
COL2A1
IGFBP5
THBS3
COL15A1
PLA2G2A
ADAMTS5
COL1A2
AEBP1
MYOC
CCN1
COL5A3
ELN
ANGPTL4
Proteomics Log2FC to DMSO
RNA-seq Log2FC to DMSO
6
3
0
-3
-6
-4
-2
0
2
4

Effects of GDF15 treatment on gene expression in normal human chondrocytes

To examine the potential effects of GDF15 release from senescent chondrocytes on non-senescent neighboring cells, we treated human articular chondrocytes isolated from normal cartilage with GDF15 at 1ng/ml which is in the range found in OA patient's serum (1–2 ng/ml) and OA synovial fluid (200 pg/ml–1 ng/ml)[23]. We also tested a 10 ng/ml concentration, which might occur locally in the tissue microenvironment. RNA from both treatment concentrations was collected at early (6 hours) and overnight (18 hours) response time points (Fig. 6A). Under 1 ng/ml GDF-15 concentrations, the early response showed a very modest decrease in inflammatory-related genes, *IL6*, *CXCL6* and *CCL20* and a modest increase in Zinc finger proteins including *ZNF544*, *ZNF442*, and *ZNF449* (Fig. 6B). The overnight response showed a modest decrease in *NTRK3* and *RNF128* and modest increase in *IFI44L* and *ITGA4* (Fig. 6C). Hallmarks revealed enrichment for upregulated pathways like apical junction, G2M checkpoint and E2F targets, and downregulated pathways including TNFA signaling, inflammatory response, and IL6 /JAK /STAT3 signaling for both time points (Fig. 6 D-E). For the physiologic dose of GDF15 [1ng/ml], we looked at genes of interest by calculating a fold-change analysis of the total RNA counts; *IL-6* and *CXCL8* showed a consistent decrease in expression across all treatments and time points, while *ACAN* and *MMP1* showed no change in response to GDF15 (Fig. 6F). *CDKN1A* and *CDKN2A* did not change, while *MKI67* and *TOP2A* showed a more consistent increase across donors at the late time point (Fig. 6G). *GDF15* expression decreased while *GDF5* expression increased at the early time point (Fig. 6H).

The 10 ng/ml dose of GDF15 showed a modest early decrease in *IL6*, *CCL20*, *CCL7*, and *GDF15*, and a modest increase in *ZNF544* and *ZNF442* (Fig. S6B). The overnight response showed a modest decrease in *IFI44L* and EFHC2 and a modest increase in *SAMSN1* and *ITGA4 (*Fig. S6C). Hallmarks differed at both time points, but estrogen response and coagulation were upregulated, and interferon gamma signaling was downregulated at both time points (Fig. S6D-E). Overnight differential gene expression was very similar to the early-response genes; however, inflammatory-related proteins were not downregulated to the same extent as in the early response and GDF15 and GDF5 showed similar trends at early timepoints under both concentrations (Fig. S6F-H).


A
Normal chondrocytes (n=4)
GDF-15 [1 ng/ml]
RNA
RNA-seq
0 hours
6 hours
18 hours
Early response
Overnight response
B
Early response (6 hours)
-log10(p-value)
Log2FoldChange
C
Overnight response (18 hours)
-log10(p-value)
Log2FoldChange
D
Hallmarks
APICAL JUNCTION
ESTROGEN RESPONSE LATE
MYOGENESIS
G2M CHECKPOINT
KRAS SIGNALING DN
ESTROGEN RESPONSE EARLY
E2F TARGETS
WNT BETA CATENIN SIGNALING
BILE ACID METABOLISM
HEME METABOLISM
TNFA SIGNALING VIA NFKB
MYC TARGETS V1
INFLAMMATORY RESPONSE
MTORC1 SIGNALING
COMPLEMENT
INTERFERON GAMMA RESPONSE
MYC TARGETS V2
INTERFERON ALPHA RESPONSE
UNFOLDED PROTEIN RESPONSE
IL6 JAK STAT3 SIGNALING
Normalized Enrichment Score
E
Hallmarks
INTERFERON ALPHA RESPONSE
G2M CHECKPOINT
E2F TARGETS
MYC TARGETS V1
OXIDATIVE PHOSPHORYLATION
INTERFERON GAMMA RESPONSE
HEDGEHOG SIGNALING
MYC TARGETS V2
ESTROGEN RESPONSE LATE
APICAL JUNCTION
KRAS SIGNALING UP
TNFA SIGNALING VIA NFKB
UV RESPONSE DN
IL6 JAK STAT3 SIGNALING
WNT BETA CATENIN SIGNALING
TGF BETA SIGNALING
NOTCH SIGNALING
HEME METABOLISM
APICAL SURFACE
ESTROGEN RESPONSE EARLY
Normalized Enrichment Score
F
IL6
p = 0.0582
p = 0.0301
CXCL8
p = 0.0100
p = 0.0246
ACAN
p = 0.1731
p = 0.9486
MMP1
p = 0.6185
p = 0.8721
mRNA expression Fold change to control
Early response
Late response
G
CDKN1A
p = 0.1114
p = 0.2438
CDKN2A
p = 0.9020
p = 0.9316
TOP2A
p = 0.2428
p = 0.4640
MKI67
p = 0.3201
p = 0.8174
H
GDF15
p = 0.1483
p = 0.9931
GDF5
p = 0.4362
p = 0.3648
Control
1ng/mL GDF15

Discussion

Cellular senescence is increasingly recognized as a potential contributor to osteoarthritis pathogenesis through accumulation of senescent chondrocytes and their altered secretory state [24,25], yet defining senescence in primary human chondrocytes remains challenging. Cell culture studies often investigate mechanisms underlying senescence and the SASP but are limited by the low numbers of enriched senescent cells. This study shows that oxygen availability strongly influences the enrichment of the senescence-associated phenotype in human osteoarthritic chondrocytes, with cells cultured under conventional hyperoxic conditions exhibiting a more pronounced secretory response than cells maintained at physiologic oxygen tension. Across both conditions, senescence enrichment with doxorubicin induced transcriptional changes and altered the protein composition of conditioned media, and the magnitude of these responses differed with oxygen tension. Notably, senescence scoring using multiple transcriptional programs showed that the more “senescent” dataset depends on the program used. Together, these findings highlight that oxygen tension is an important determinant of how senescence is manifested in human chondrocytes and suggest that physiologic culture conditions should be considered when defining and interpreting senescence-associated phenotypes in OA.

Our results raise an important question: how should senescence be defined in this cell type? Our comparison of commonly used markers demonstrated that no single measure consistently captured the senescence-associated state. In particular, p16 and p21 provided more consistent evidence of doxorubicin-induced senescence than SA-β-gal, which showed greater donor variability and higher detectable baseline activity.

Consistent with cellular heterogeneity, transcriptomic analyses revealed both shared and oxygen-specific responses. *TNFRSF10C* was significantly upregulated, and *KIF20A* was significantly downregulated under both oxygen tensions. In contrast, genes such as *SDC1*, *PENK*, and *IFI6* were uniquely upregulated under hyperoxia, whereas *KRT17*, *PAPPA*, and *APOD* were uniquely upregulated under normoxia. *PAPPA* is of particular interest since it has been linked to senescence[26] and is a risk gene for OA[27,28] but its exact role remains to be delineated. Pathway enrichment further showed that the biological interpretation of these transcriptional changes depended on the database used. Hallmark analysis consistently identified activation of the p53 pathway and reduced mitotic activity under both oxygen tensions, while Reactome detected the SASP process only under hyperoxia. This again emphasizes the importance of integrating multiple complementary measures and using multiple enrichment databases when characterizing senescence in OA chondrocytes. Our findings also demonstrated that molecules detected at the protein secretion and gene expression levels were not always concordant. Secreted proteins identified by proteomics were more informative for SASP identification, whereas transcriptional data were better suited to enrichment analysis and senescence scoring.

We applied different senescence scoring programs to assess whether doxorubicin-induced transcriptional changes were consistent with senescence. SenCID categorized the chondrocytes as belonging to the SID3 category, consistent with a prior study[14], and doxorubicin-treated samples generally showed higher SID3 senescence scores. Normoxia showed greater separation among control and treated samples in both SenCID and DeepScence, whereas DeepScence provided greater separation

under hyperoxia. These findings suggest that senescence scoring is not represented by a single conserved transcriptional scoring program and that individual algorithms may capture distinct aspects of the phenotype. Although our senescence scoring analysis (Supplementary Table 5) yields a 47-gene list primarily derived from doxorubicin-induced senescence in OA chondrocytes, it highlights that genes contributing to the senescent phenotype in chondrocytes may differ from those commonly identified in other cell types. This is consistent with findings that senescence signatures can be tissue- and disease-context dependent, with specific cell types potentially exhibiting distinct transcriptional programs associated with both senescence and disease pathology. The 47 genes identified in our analysis included multiple genes known to have altered expression in OA, including collagens, TIMPs, MMPs, IGFBPs, and aggrecan, further supporting the relevance of senescence to the development of OA. However, it is important to note that OA cells that are not senescent also contribute to the production of OA mediators in response to other stressors such as mechanical and metabolic stress or in response to matrix damage.

GDF15 emerged as a particularly prominent SASP factor in our datasets and has been consistently represented in established senescence resources using cells from other tissues, including the SenMayo and SenNet SASP databases[10,20]. Despite its strong association with the senescent phenotype, treatment of normal chondrocytes with physiologically relevant concentrations of GDF15 produced limited responses, with no evidence of direct induction of senescence-associated markers. Downregulation of *IL6* and *CXCL8*, and pathways associated with TNFα signaling and the inflammatory response, suggests that GDF-15's effects are more anti-inflammatory. Similar

chondrocyte studies using higher concentrations of GDF-15 reported modest effects, suggesting that GDF15's biological activity may depend on both dose and duration of exposure[23]. The GDNF family receptor alpha-like protein (GFRAL) is considered the primary receptor for GDF15, and its function has been related to its cachexia and anorectic effects[29]. GDF15 has also been reported to interact with TGF-β receptor pathways[30], raising the possibility that its effects on chondrocytes may involve TGF-β signaling. Sustained TGF-β signaling has been implicated in aging and senescence-associated disease [31]; therefore, chronic exposure to GDF15 may produce effects not captured by the acute treatment used in the present study. Future studies using prolonged GDF15 exposure, particularly in combination with a senescence-inducing stressor, will be important to determine whether GDF15 functions primarily as a marker of the senescent secretome or can actively contribute to the establishment or maintenance of senescence.

In conclusion, our findings on differences across senescence markers, transcriptional programs, proteomics, and senescence scoring approaches further highlight the heterogeneity of the senescent phenotype and the limitations of relying on a single marker or scoring system. The 47 genes shared across multiple senescence-scoring approaches, including multiple OA-associated genes, further suggest that senescence signatures may be disease context-dependent and provide a potential starting point for developing a chondrocyte-relevant approach to assess senescence in OA. Despite GDF15 being a prominent senescence-associated secreted factor in our datasets, short-term treatment produced limited effects in normal chondrocytes, suggesting that its biological activity may depend on exposure duration, cellular context,

or interactions with other SASP factors. Together, these findings demonstrate the value of integrating senescence markers, transcriptomic scoring, and secretome profiling to both assess senescence induction and identify candidate genes and factors that may be particularly relevant to OA chondrocytes. This integrated approach may help define more disease-specific features of senescence and improve how senescence is assessed in OA.

Ethics declarations

Ethics approval and consent to participate

The use of de-identified cadaveric and surgical waste tissues was approved by the UNC Institutional Review Board (IRB #14-0189) and determined not to constitute human subjects research.

Consent for publication

Not applicable.

Competing interests

The authors declare no competing interests.

Funding

This study was supported by the National Institute on Aging: R01, AG044034 (RFL), R01AG081734 (BOD), and UNC-CH Summer Research Training in Aging for Medical Students: 5-T35-AG038047, and the National Cancer Institute: P30CA012197.

The content is solely the responsibility of the authors and does not necessarily represent the official views of the National Institutes of Health.

Acknowledgements

The authors wish to acknowledge the support of the Proteomics and Metabolomics Shared Resource at Atrium Health Wake Forest Baptist Comprehensive Cancer Center. We thank Dr. Phil Coryell for input on data analysis and Haroon Giliani for technical assistance. We also thank Dr. Sarah Rice, University of Manchester, for providing technical advice.

Author contributions

J.G.F.D., M.J.P., A.P., S.B., J.S., C.W.O., H.P., J.L., D.H.P., B.O.D., and R.F.L. contributed to acquisition, analysis, and interpretation of the data. J.G.F.D., M.J.P., A.P., B.O.D., and R.F.L. contributed to conception and design of the work. J.G.F.D. and R.F.L. drafted the manuscript. J.G.F.D. agreed to be accountable for all aspects of the presented work. All authors reviewed the draft and approved the final version of the article.

References

1. Katz JN, Arant KR, Loeser RF. Diagnosis and Treatment of Hip and Knee Osteoarthritis: A Review. JAMA. 2021;325:568–78. https://doi.org/10.1001/jama.2020.22171

2. Tang S, Zhang C, Oo WM, Fu K, Risberg MA, Bierma-Zeinstra SM, et al. Osteoarthritis. Nat Rev Dis Primer. Nature Publishing Group; 2025;11:10. https://doi.org/10.1038/s41572-025-00594-6

3. Gorgoulis V, Adams PD, Alimonti A, Bennett DC, Bischof O, Bishop C, et al. Cellular Senescence: Defining a Path Forward. Cell. Elsevier; 2019;179:813–27. https://doi.org/10.1016/j.cell.2019.10.005

4. López-Otín C, Blasco MA, Partridge L, Serrano M, Kroemer G. Hallmarks of aging: An expanding universe. Cell. Elsevier; 2023;186:243–78. https://doi.org/10.1016/j.cell.2022.11.001

5. Lopes-Paciencia S, Saint-Germain E, Rowell M-C, Ruiz AF, Kalegari P, Ferbeyre G. The senescence-associated secretory phenotype and its regulation. Cytokine. 2019;117:15–22. https://doi.org/10.1016/j.cyto.2019.01.013

6. Suryadevara V, Farzad N, Yang M, Xu K, Tsankov A, Thompson RC, et al. Charting human cellular senescence in aging and disease. Cell. Elsevier; 2026;189:3501–5. https://doi.org/10.1016/j.cell.2026.05.028

7. Li S, Agudelo Garcia PA, Aliferis C, Becich MJ, Calyeca J, Cosgrove BD, et al. Advancing biological understanding of cellular senescence with computational multiomics. Nat Genet. Nature Publishing Group; 2025;57:2381–94. https://doi.org/10.1038/s41588-025-02314-y

8. Jenei-Lanzl Z, Zaucke F. Osteoarthritis year in review 2024: Biology. Osteoarthritis Cartilage. Elsevier; 2025;33:58–66. https://doi.org/10.1016/j.joca.2024.10.008

9. Diekman BO, Loeser RF. Aging and the emerging role of cellular senescence in osteoarthritis. Osteoarthritis Cartilage. Elsevier; 2024;32:365–71. https://doi.org/10.1016/j.joca.2023.11.018

10. Suryadevara V, Hudgins AD, Rajesh A, Pappalardo A, Karpova A, Dey AK, et al. SenNet recommendations for detecting senescent cells in different tissues. Nat Rev Mol Cell Biol. 2024;25:1001–23. https://doi.org/10.1038/s41580-024-00738-8

11. Zhou S, Cui Z, Urban JPG. Factors influencing the oxygen concentration gradient from the synovial surface of articular cartilage to the cartilage-bone interface: a modeling study. Arthritis Rheum. 2004;50:3915–24. https://doi.org/10.1002/art.20675

12. Kciuk M, Gielecińska A, Mujwar S, Kołat D, Kałuzińska-Kołat Ż, Celik I, et al. Doxorubicin—An Agent with Multiple Mechanisms of Anticancer Activity. Cells. Multidisciplinary Digital Publishing Institute; 2023;12:659. https://doi.org/10.3390/cells12040659

13. Kirsch V, Ramge J-M, Schoppa A, Ignatius A, Riegger J. In Vitro Characterization of Doxorubicin-Mediated Stress-Induced Premature Senescence in Human Chondrocytes. Cells. 2022;11:1106. https://doi.org/10.3390/cells11071106

14. Tao W, Yu Z, Han J-DJ. Single-cell senescence identification reveals senescence heterogeneity, trajectory, and modulators. Cell Metab. Elsevier; 2024;36:1126-1143.e5. https://doi.org/10.1016/j.cmet.2024.03.009

15. Wang J, Zhou X, Yu P, Yao J, Guo P, Xu Q, et al. A transcriptome-based human universal senescence index (hUSI) robustly predicts cellular senescence under various conditions. Nat Aging. 2025;5:1159–75. https://doi.org/10.1038/s43587-025-00886-2

16. Qu Y, Ji B, Dong R, Gu L, Chan C, Xie J, et al. Single-cell and spatial detection of senescent cells using DeepScence. Cell Genomics [Internet]. Elsevier; 2025 [cited 2026 Aug 31];5. https://doi.org/10.1016/j.xgen.2025.101035

17. Saul D, Kosinsky RL, Atkinson EJ, Doolittle ML, Zhang X, LeBrasseur NK, et al. A new gene set identifies senescent cells and predicts senescence-associated pathways across tissues. Nat Commun. Nature Publishing Group; 2022;13:4827. https://doi.org/10.1038/s41467-022-32552-1

18. Miao MZ, Su QP, Cui Y, Bahnson EM, Li G, Wang M, et al. Redox-active endosomes mediate α5β1 integrin signaling and promote chondrocyte matrix metalloproteinase production in osteoarthritis. Sci Signal. 2023;16:eadf8299. https://doi.org/10.1126/scisignal.adf8299

19. Reed KSM, Ulici V, Kim C, Chubinskaya S, Loeser RF, Phanstiel DH. Transcriptional response of human articular chondrocytes treated with fibronectin fragments: an in vitro model of the osteoarthritis phenotype. Osteoarthritis Cartilage. 2021;29:235–47. https://doi.org/10.1016/j.joca.2020.09.006

20. Saul D, Kosinsky RL, Atkinson EJ, Doolittle ML, Zhang X, LeBrasseur NK, et al. A new gene set identifies senescent cells and predicts senescence-associated pathways

across tissues. Nat Commun. Nature Publishing Group; 2022;13:4827. https://doi.org/10.1038/s41467-022-32552-1

21. Kudlova N, De Sanctis JB, Hajduch M. Cellular Senescence: Molecular Targets, Biomarkers, and Senolytic Drugs. Int J Mol Sci. 2022;23:4168. https://doi.org/10.3390/ijms23084168

22. Freund A, Laberge R-M, Demaria M, Campisi J. Lamin B1 loss is a senescence-associated biomarker. Mol Biol Cell. 2012;23:2066–75. https://doi.org/10.1091/mbc.E11-10-0884

23. Marques SS, Liebaug A, Maurer S, Rothenbacher D, Brenner RE, Riegger J. Growth/Differentiation Factor 15 Promotes a Pro-Regenerative Response in Chondrocytes Upon Cartilage Injury. MedComm. 2025;6:e70484. https://doi.org/10.1002/mco2.70484

24. Huang K, Cai H. The role of chondrocyte senescence in osteoarthritis pathogenesis and therapeutic implications. Exp Gerontol. 2025;208:112828. https://doi.org/10.1016/j.exger.2025.112828

25. Loeser RF. Aging and Osteoarthritis: The Role of Chondrocyte Senescence and Aging Changes in the Cartilage Matrix. Osteoarthr Cartil OARS Osteoarthr Res Soc. 2009;17:971–9. https://doi.org/10.1016/j.joca.2009.03.002

26. Bi S, Jiang X, Ji Q, Wang Z, Ren J, Wang S, et al. The sirtuin-associated human senescence program converges on the activation of placenta-specific gene PAPPA. Dev Cell. Elsevier; 2024;59:991-1009.e12. https://doi.org/10.1016/j.devcel.2024.02.008

27. Kramer NE, Byun S, Coryell P, D'Costa S, Thulson E, Kim H, et al. Response eQTLs, chromatin accessibility, and 3D chromatin structure in chondrocytes provide mechanistic insight into osteoarthritis risk. Cell Genomics. 2025;5:100738. https://doi.org/10.1016/j.xgen.2024.100738

28. Bittner N, Shi C, Zhao D, Ding J, Southam L, Swift D, et al. Primary osteoarthritis chondrocyte map of chromatin conformation reveals novel candidate effector genes. Ann Rheum Dis. 2024;83:1048–59. https://doi.org/10.1136/ard-2023-224945

29. Hüllwegen M, Kleinert M, Haehling S von, Fischer A. GDF15: from biomarker to target in cancer cachexia. Trends Cancer. Elsevier; 2025;11:1093–105. https://doi.org/10.1016/j.trecan.2025.06.007

30. Wang D, Wei X, Geng X, Li P, Li L. GDF15 enhances proliferation of aged chondrocytes by phosphorylating SMAD2. J Orthop Sci Off J Jpn Orthop Assoc. 2022;27:249–56. https://doi.org/10.1016/j.jos.2020.12.004

31. Tominaga K, Suzuki HI. TGF-β Signaling in Cellular Senescence and Aging-Related Pathology. Int J Mol Sci. 2019;20:5002. https://doi.org/10.3390/ijms20205002

Figure legends

Fig. 1. OA articular chondrocytes express senescent signatures in response to doxorubicin. (A) Schematic timeline of doxorubicin treatment and collection of samples, created with BioRender. (B) Fold-change gene expression by qPCR in chondrocytes treated with 1 μM doxorubicin for *CDKN1A*, *CDKN2A*, *KI67*, *LMNB1*, *COL2A1*, *IL6*, and

MMP13; statistical test: one-sample t-test; donors: n=8. (C) Immunofluorescence images of OA chondrocytes with specific antibodies for p16 (Cy5), p21 (RFP), and DAPI (blue) nuclear stain; scale bar: 100 μm. (D) Immunofluorescence images showing localization of p16 and p21 within the nuclear compartment; scale bar: 20 μM. (E) Mean fluorescence intensity (MFI) of p21 and p16 within the nucleus assessed by quantification; statistical test: paired t-test; donors: n=4. DMSO: dimethyl sulfoxide; Doxo: doxorubicin. Each data point represents the mean of all analyzed cells for an individual donor (e.g. >50 cells per donor). Error bars indicate standard deviation.

Fig. 2. OA chondrocyte senescence enrichment under different oxygen tensions alters gene expression. (A) Schematic timeline of doxorubicin treatments on OA chondrocytes cultured under hyperoxia and normoxia, created with BioRender. (B) PCA plot demonstrating variance across principal components for hyperoxia, hypoxia, doxorubicin, and DMSO treatments based on chondrocyte RNA-seq gene expression. (C) Fold-change gene expression by qPCR in chondrocytes for *CDKN1A* and *CDKN2A*; statistical test: one-sample t-test. (D) Volcano plot of differentially expressed genes by RNAseq in chondrocytes under hyperoxia and treatment with 1 μM doxorubicin, and (E) Volcano plot of RNA-seq results from chondrocytes in normoxia treated with 0.5 μM doxorubicin. (F) Top 10 upregulated and downregulated Hallmarks for hyperoxia with 1 μM doxorubicin and (G) Top 10 upregulated and downregulated Hallmarks under normoxia with 0.5 μM doxorubicin.

Fig. 3. Senescence scoring of chondrocyte gene expression datasets. (A) Schematic diagram of the methodology used for senescence scoring with SenCID, hUSI, and DeepScence. For panels B-E, senescent samples are categorized as having scores of greater than 0.5, and non-senescent samples are categorized below 0.5. (B) Distribution of senescence scores for all chondrocyte treatments in each SID category of 1-6. (D) Individual SID3 scores based on different treatments. (C) tSNE plot; colorimetric scale ranges from 0 (purple) to 1 (yellow). (E) Individual hUSI scores for all chondrocyte treatments. Error bars indicate standard deviation. (F) Venn diagram comparison of all 125 SenMayo genes and top 125 ranked genes using hUSI and DeepScence. Genes shared between 2 or more groups are circled in red, total of 47 genes. (G) Heatmap of 47 genes shared across the Venn diagram in panel G. Dimethyl sulfoxide: DMSO; Doxo: doxorubicin.

Figure 4. Proteomics analysis of conditioned medium from senescent osteoarthritic chondrocytes. (A) Distribution plot of all secreted proteins detected under each condition. (B) Venn diagram showing the number of secreted proteins detected under each condition, with the top 10 increased and decreased secreted proteins common to both conditions. (C) Heatmap of the highest and lowest regulated top 25 proteins in cells treated with doxorubicin under hyperoxia. (D) Heatmap of the 25 highest and lowest proteins in cells treated with doxorubicin under normoxia. (E) Bar graphs of OA-secreted matrix-related proteins under hyperoxia and normoxia. (F) Schematic diagram of proteins detected from SenNet and CoreScence. (G) Bar graph of log2 fold change

relative to the DMSO control of shared proteins from the diagram in panel F. Error bars indicate standard deviation.

Figure 5. Integration of RNA-seq and proteomics analysis of senescent OA chondrocytes. Quadrant diagrams of proteomics and transcriptomic data that matched across both datasets for: (A) RNAseq and proteomics data from cells cultured under hyperoxia. (B) RNAseq and proteomics data from cells cultured under normoxia. (-/+) indicates negative RNA-seq log2FC and positive proteomics log2FC regulation. (+/+) indicates positive RNA-seq log2FC and positive proteomics log2FC regulation. (-/-) indicates negative RNA-seq log2FC and negative proteomics log2FC regulation. (+/-) indicates positive RNA-seq log2FC and negative proteomics log2FC regulation.

Figure 6. Recombinant human GDF15 treatment effects on human chondrocytes. Volcano plot of differentially expressed genes up- or down-regulated in chondrocytes (n=4): (A) 6-hour (early response) and (B) 18-hour (late response) of normal human chondrocytes to 1 ng/ml GDF-15. Top 10 upregulated and downregulated Hallmarks for (C) 6-hour (early response) and (D) 18-hour (late response) of normal human chondrocytes to 1 ng/ml GDF-15. Bar graphs of fold-change gene expression of (E) inflammatory and matrix-related genes – *IL6*, *CXCL8*, *ACAN,* and *MMP1*; (F) cell cycle and proliferation markers – *CDKN1A*, *CDKN2A*, *MKI67*, *TOP2A*; and (G) *GDF15* and *GDF5.*

856

857

858

859

Supplementary Files

This is a list of supplementary files associated with this preprint. Click to download.

- SupplementalTablesSenescence.xlsx
- SupplementaryMethods.docx
- SupplementarysenescencePaperFigs100826.pdf